

CFNet: Cascade Fusion Network for Dense Prediction

Gang Zhang¹ Ziyi Li⁴ Jianmin Li¹ Xiaolin Hu^{1,2,3*}

¹Department of Computer Science and Technology, Institute for AI, BNRist, THU-Bosch JCML Center, Tsinghua University, Beijing 100084, China

²Tsinghua Laboratory of Brain and Intelligence (THBI), IDG/McGovern Institute for Brain Research, Tsinghua University, Beijing 100084, China

³Chinese Institute for Brain Research (CIBR), Beijing 100010, China

⁴Huazhong University of Science and Technology, Wuhan 430074, China

zhang-g19@mails.tsinghua.edu.cn, liziyi@hust.edu.cn, {lijianmin, xlhu}@mail.tsinghua.edu.cn

Abstract

Multi-scale features are essential for dense prediction tasks, including object detection, instance segmentation, and semantic segmentation. Existing state-of-the-art methods usually first extract multi-scale features by a classification backbone and then fuse these features by a lightweight module (e.g. the fusion module in FPN). However, we argue that it may not be sufficient to fuse the multi-scale features through such a paradigm, because the parameters allocated for feature fusion are limited compared with the heavy classification backbone. In order to address this issue, we propose a new architecture named Cascade Fusion Network (CFNet) for dense prediction. Besides the stem and several blocks used to extract initial high-resolution features, we introduce several cascaded stages to generate multi-scale features in CFNet. Each stage includes a sub-backbone for feature extraction and an extremely lightweight transition block for feature integration. This design makes it possible to fuse features more deeply and effectively with a large proportion of parameters of the whole backbone. Extensive experiments on object detection, instance segmentation, and semantic segmentation validated the effectiveness of the proposed CFNet. Codes will be available [here](#).

1. Introduction

In the past few years, convolutional neural networks (CNNs) and transformer-based networks have achieved promising results in many computer vision tasks including image classification, object detection, semantic segmentation, *etc.* For the image classification task, most popular

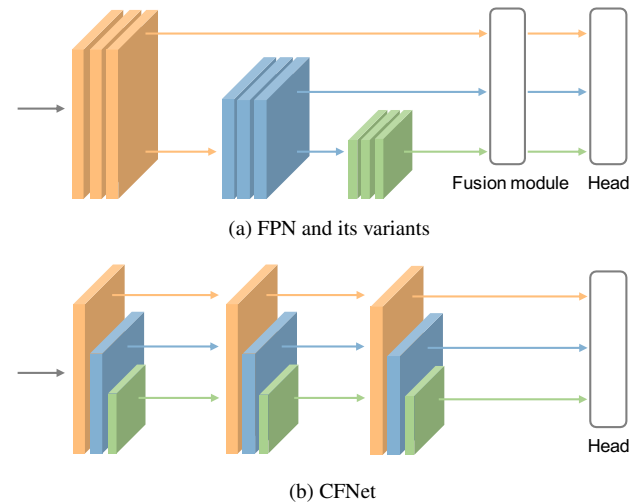


Figure 1. Two paradigms to extract multi-scale features: (a) FPN and its variants, (b) our proposed CFNet. Each cube denotes feature maps of a specific scale, and the stacked cubes are connected sequentially. Cubes with the same color stand for feature maps with the same spatial size. The arrows denote information flows.

CNNs [1–5] and recently developed transformer-based networks [6–9] usually follow a sequential manner in the design of architecture, *i.e.* gradually reduce the spatial size of feature maps, and perform prediction based on the coarsest scale of features. However, for many dense prediction tasks, such as object detection and instance segmentation, multi-scale features are needed to handle objects of different scales. Obtaining multi-scale features and integrating them effectively is critical for the success of these tasks [10–14].

Feature pyramid network (FPN) and its variants [14–20] are the widely used models proposed for multi-scale feature extraction and fusion. As illustrated in Figure 1 (a), these models usually consist of a heavy classification back-

*Corresponding Author

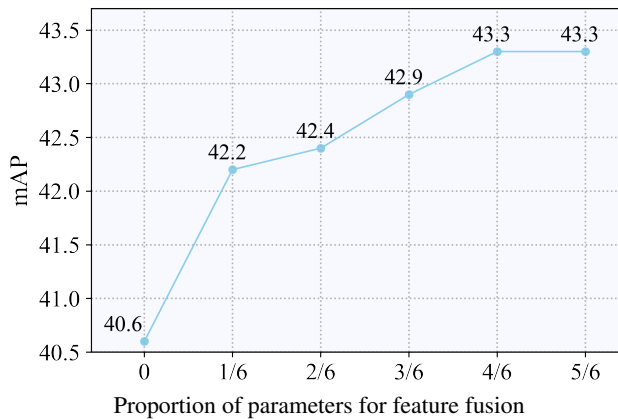


Figure 2. Comparison among models with different proportions of parameters allocated for feature fusion.

bone for extracting multi-scale features and a lightweight fusion module for fusing these features. However, we argue that using such a paradigm might be insufficient for fusing multi-scale features, because the parameters allocated for feature fusion are limited compared with the heavy classification backbone. For example, considering a FPN built based on the backbone ConvNeXt-S [5], the ratio of parameters of the fusion module to the backbone is smaller than 10%. *We suppose that allocating a larger proportion of parameters for feature fusion can achieve better performance.*

Given a fixed computational budget, if we want to allocate more parameters for feature fusion, an intuitive way is to use a smaller backbone and scale up the fusion module. However, using a smaller backbone means that the entire model can benefit less from large-scale pre-training (e.g. the ImageNet classification pre-training) which is critical for downstream tasks with limited training data. *So how can we allocate more parameters to achieve feature fusion, while keeping a simple model architecture that can still benefit from large-scale pre-training to the greatest extent?*

Let’s first review the fusion module of FPN. In order to fuse multi-scale features, the features from adjacent levels are first integrated by performing element-wise addition, then a single 3×3 convolution is used to transform the summed features. We name these two steps as *feature integration* and *feature transformation* to compose the feature fusion. It is obvious that we can stack more convolutions to transform the integrated features, but it introduces more parameters, leaving fewer parameters for the backbone. Thinking from another perspective, we further ask *whether the feature integration operation can be inserted into the backbone so that all the parameters after it can be utilized to transform the integrated features.*

In this work, we try to answer the above questions. We propose a new architecture named Cascade Fusion Network

(CFNet) for dense prediction. Figure 1(b) illustrates the information flows of CFNet. It can be regarded as the results of reorganizing the connections among features of different scales. Figure 3 shows the architecture of CFNet. Based on the high-resolution features extracted by a stem and several blocks, M cascaded CFNet stages are introduced to generate multi-scale features. All stages share the same structure, but their sizes can be different. Specifically, each stage includes a sub-backbone for extracting multi-scale features and an extremely lightweight transition block for *integrating* these features. In this way, we insert the feature integration operation into the backbone so that the integrated features can be *transformed* by all stages after the transition block. In other words, all parameters after the transition block can be utilized for feature fusion. Besides, the experiments we conducted on the image classification task demonstrate that CFNet can still benefit from large-scale pre-training due to its simple architecture.

Based on the proposed CFNet, we conducted a set of experiments to validate our supposition. We define the *proportion of parameters for feature fusion* in CFNet as the ratio of parameters of all stages after the *first* transition block to the whole backbone. The results in Figure 2 show that the detection performance is gradually improved with more parameters allocated for feature fusion, which validates our supposition. Please refer to Section 4.1 for more details.

We conducted extensive experiments on three popular dense prediction tasks. On the COCO *val 2017* for object detection and instance segmentation, CFNet outperformed its baselines, *i.e.* the Swin Transformer [6] and ConvNeXt [5], by 1.9-2.9 box AP and 1.2-1.8 mask AP based on the popular RetinaNet [4] and Mask R-CNN [10]. On the ADE20k for semantic segmentation, CFNet outperformed its baseline by 0.8-2.2 mIoU based on the powerful UperNet [13]. These results indicate the strong performances of CFNet and encourage the community to rethink the widely used model design principle for dense prediction tasks.

2. Related work

2.1. Backbone designs for dense prediction

For dense prediction tasks, most existing works adopt the strategy of combining an image classification network and a feature fusion module to extract and fuse multi-scale features. However, directly applying the pre-designed classification network to dense prediction tasks may be sub-optimal. Therefore, designing task-friendly backbones for dense prediction has aroused great interest [21–29]. In order to acquire high-resolution features with strong semantics, both UNet [21] and SegNet [22] adopt a similar U-shape structure with skip connections for medical image segmentation. Hourglass [23] introduces a convolutional network architecture which uses repeated bottom-up and

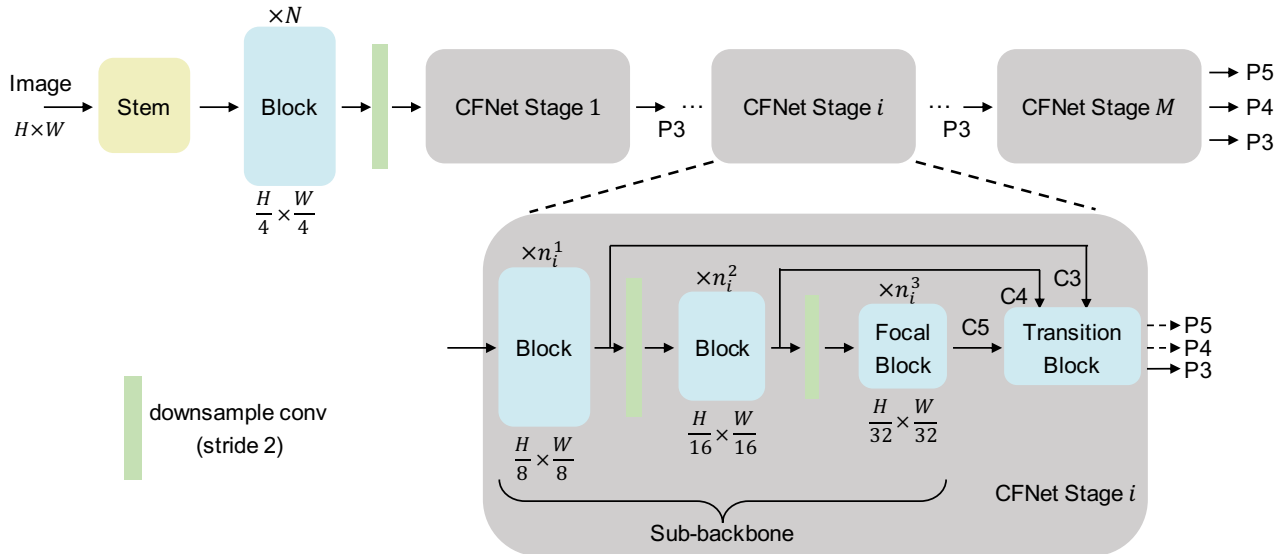


Figure 3. Architecture of CFNet. The input image with spatial size of $H \times W$ is first fed into a stem and N consecutive blocks to extract high-resolution features with spatial size of $\frac{H}{4} \times \frac{W}{4}$. Then, those features are fed into M cascaded stages to extract multi-scale features. Each stage outputs the fused features P3, P4, P5 with a stride 8, 16, 32, but only the P3 are fed into the later stage. Note that only the stem and the ‘downsample conv’ reduce the spatial size of features. $\times n_i^k$ ($k=1,2,3$) denotes n_i^k consecutive blocks are applied.

top-down processing for the task of human pose estimation. HRNet [25] maintains high-resolution features through the whole forwarding process, and the resulting representations perform well on semantic segmentation and human pose estimation. SpineNet [26] introduces neural architecture search (NAS) [30] to learn scale-permuted backbone for object detection. GiraffeDet [29] adopts a lightweight backbone combined with a heavy fusion module to encourage dense information exchange among features of different scales. CBNet [27] assembles multiple identical backbones by introducing composite connections between adjacent backbones. And DetectoRS [28] directly stacks several FPNs to enhance the multi-scale features. Different from these methods, we introduce several cascaded stages to extract and integrate multi-scale features iteratively based on the extracted high-resolution features in CFNet.

2.2. Multi-scale feature fusion

As the low-level features generated by conventional classification networks are semantically weak, those multi-scale features are not suitable for downstream dense prediction tasks. To address this issue, many methods [14–18, 31–33] have been proposed for multi-scale feature fusion. For semantic segmentation, DeeplabV3+ [31] fuses low-level features with the semantically strong high-level features obtained by atrous spatial pyramid pooling. ESeg [32] adopts a much richer multi-scale feature space and uses a powerful feature fusion network to fuse features. For object detection, FPN [14] introduces a top-down pathway to sequen-

tially combine high-level features with low-level features. PANet [15] further adds another bottom-up pathway to shorten the information pathway between low-level features and topmost features. NAS-FPN [16] fuses multi-scale features by repeated fusion stages searched by NAS [30]. EfficientDet [17] adopts a weighted bi-directional feature pyramid network with compound scaling rule to achieve easy and fast multi-scale feature fusion. A²-FPN [18] improves multi-scale feature learning through attention-guided feature aggregation. All above methods rely on a heavy classification backbone to extract multi-scale features, and then fuses the features with a lightweight fusion module. However, the parameters of the fusion module are limited compared with the classification backbone. In contrast, we propose an extremely lightweight transition block, and insert it into the backbone. In this way, all stages after the transition block can be used to fuse the integrated multi-scale features.

3. Method

3.1. Overall architecture

An overview of the CFNet architecture is presented in Figure 3. An input RGB image with spatial size of $H \times W$ is fed into a stem and N consecutive blocks to extract high-resolution features with spatial size of $\frac{H}{4} \times \frac{W}{4}$. The stem consists of two 3×3 convolutions with a stride of 2, and each is followed by a LayerNorm [34] layer and a GELU [35] unit. The block in CFNet can be any designs proposed in previous works, *e.g.* the ResNet bottleneck [4], the Con-

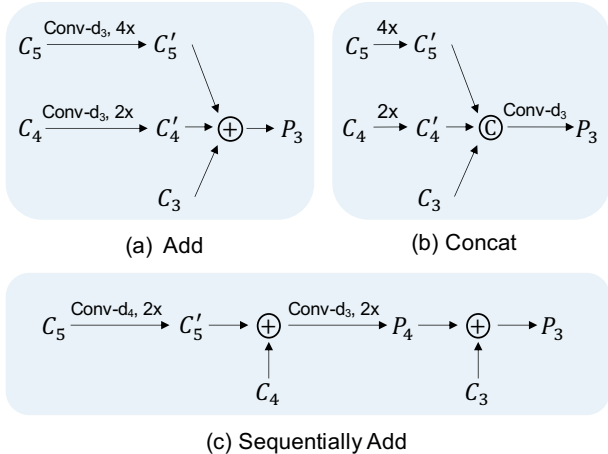


Figure 4. Three designs of the transition block. Given the C_3 , C_4 , C_5 as inputs, the transition block outputs features P_3 , P_4 , P_5 . If there is no P_4/P_5 in a specific design, the C_4/C_5 is the output P_4/P_5 (identity mapping). Conv-d_x denotes a 1×1 conv with output channel number of d_x , where d_x is the channel number of feature C_x . The circles with $+$ and C denote element-wise addition and concatenation operation, respectively. $2 \times$ denotes up-sampling the features with a scale factor of 2, and $4 \times$ is similar.

vNeXt block [5], the Swin Transformer block [6], etc.

Before being fed into M cascaded stages, the extracted high-resolution features are downsampled by a 2×2 convolution with a stride of 2. All stages share the same structure, but may have different sizes, *i.e.* different number of blocks. Specifically, each stage consists of a sub-backbone and an extremely lightweight transition block to extract and integrate features of different scales. Here, we define a block group in each stage as the union of blocks used to transform features of the same scale. n_i^1 , n_i^2 , and n_i^3 denote the number of blocks included in the three block groups of the i -th stage, respectively. In the last block group of each stage, focal blocks are applied. More details about the transition block and the focal block are introduced in Section 3.2 and Section 3.3, respectively. It is worth noting that each stage outputs features P_3 , P_4 , P_5 with a stride of 8, 16, 32, but only the P_3 are fed into the later stage. Finally, the fused features P_3 , P_4 , and P_5 output by the last stage are used by dense prediction tasks.

3.2. Transition block

The transition block is introduced to integrate features of different scales in each stage. To avoid introducing too much extra computational cost, we propose three simple designs, as shown in Figure 4. The ‘Add’ fusion first reduces the channel numbers of features C_4 and C_5 to align that of C_3 with 1×1 convolutions. Before performing element-wise addition, bilinear interpolation operations are used to align the spatial size of features. The ‘Concat’ fusion directly up-samples the features C_4 and C_5 to align the spatial

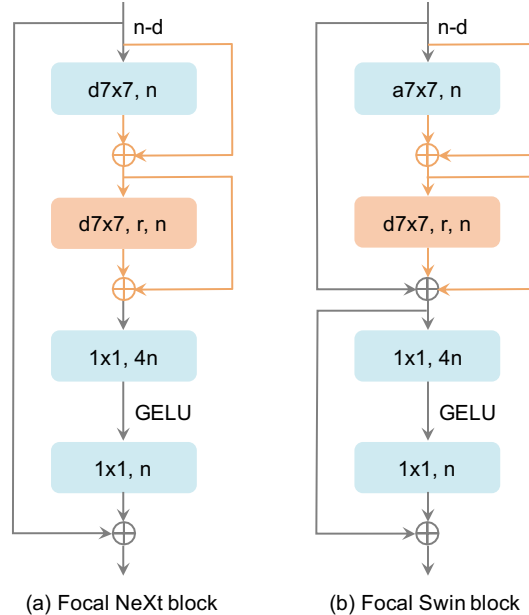


Figure 5. Two designs of the focal block. They are built based on the ConvNeXt block and the Swin Transformer block, respectively. The orange parts are operations added to the two blocks. n denotes the channel number of output features. $d7 \times 7$ denotes a 7×7 depth-wise convolution and $a7 \times 7$ denotes the window attention with a window size of 7×7 . r denotes the dilation rate of the added convolution. 1×1 denotes a 1×1 convolution. GELU [35] is an activation unit. Each $d7 \times 7$ or $a7 \times 7$ is followed by a Layer-Norm [34] layer and a GELU unit, omitted for clarity.

size of C_3 , and then concatenates these features, followed by a 1×1 convolution to reduce the channel number. The ‘Sequentially Add’ fusion up-samples and combines features of different scales sequentially. This design is similar to the fusion module in FPN, except that there are no additional convolutions to transform the summed features. The above three designs all performed well in experiments (see Table 8 in the Section 4.5 for comparison), and the ‘Sequentially Add’ fusion achieved the best results. We adopt this design in the CFNet variants (see Section 3.4) by default.

3.3. Focal block

For dense prediction tasks, it has always been a big challenge to deal with objects of various scales. A widely used solution is to generate features of different resolutions. For example, features with a stride of 8, 16, 32, 64, 128 are usually generated to detect objects of the corresponding scale in one-stage detectors [11, 12, 36, 37]. The neurons used to generate features with larger stride usually have larger receptive field. In each stage of CFNet, there are three block groups to extract features with a stride of 8, 16, 32. Ideally, we can extract the other two resolution features to integrate more feature scales, like the FPN variants [15–17]. However, it would introduce much more parameters, because the

Table 1. Detailed architecture configurations for CFNet-T (Swin), CFNet-T (NeXt), CFNet-S (NeXt). Swin and NeXt indicate using the Swin Transformer block and the ConvNeXt block to construct CFNet, respectively. The first line shows the configurations for the first N blocks. The other three lines show the configurations for the three block groups in each stage, and all stages share the same configurations.

Size	CFNet-T (Swin)	CFNet-T (NeXt)	CFNet-S (NeXt)
$\frac{H}{4} \times \frac{W}{4}$	$\begin{bmatrix} 7 \times 7 \text{ Window att, 96} \\ 1 \times 1, 384 \\ 1 \times 1, 96 \end{bmatrix} \times 3$	$\begin{bmatrix} 7 \times 7 \text{ Depth-wise conv, 96} \\ 1 \times 1, 384 \\ 1 \times 1, 96 \end{bmatrix} \times 3$	$\begin{bmatrix} 7 \times 7 \text{ Depth-wise conv, 96} \\ 1 \times 1, 384 \\ 1 \times 1, 96 \end{bmatrix} \times 3$
$\frac{H}{8} \times \frac{W}{8}$	$\begin{bmatrix} 7 \times 7 \text{ Window att, 160} \\ 1 \times 1, 640 \\ 1 \times 1, 160 \end{bmatrix} \times 2$	$\begin{bmatrix} 7 \times 7 \text{ Depth-wise conv, 192} \\ 1 \times 1, 768 \\ 1 \times 1, 192 \end{bmatrix} \times 2$	$\begin{bmatrix} 7 \times 7 \text{ Depth-wise conv, 192} \\ 1 \times 1, 768 \\ 1 \times 1, 192 \end{bmatrix} \times 2$
$\frac{H}{16} \times \frac{W}{16}$	$\begin{bmatrix} 7 \times 7 \text{ Window att, 288} \\ 1 \times 1, 1152 \\ 1 \times 1, 288 \end{bmatrix} \times 4$	$\begin{bmatrix} 7 \times 7 \text{ Depth-wise conv, 352} \\ 1 \times 1, 1408 \\ 1 \times 1, 352 \end{bmatrix} \times 4$	$\begin{bmatrix} 7 \times 7 \text{ Depth-wise conv, 352} \\ 1 \times 1, 1408 \\ 1 \times 1, 352 \end{bmatrix} \times 7$
$\frac{H}{32} \times \frac{W}{32}$	$\begin{bmatrix} 7 \times 7 \text{ Window att, 416} \\ 7 \times 7 \text{ Depth-wise conv, } r=3, 416 \\ 1 \times 1, 1664 \\ 1 \times 1, 416 \end{bmatrix} \times 2$	$\begin{bmatrix} 7 \times 7 \text{ Depth-wise conv, 512} \\ 7 \times 7 \text{ Depth-wise conv, } r=3, 512 \\ 1 \times 1, 2048 \\ 1 \times 1, 512 \end{bmatrix} \times 2$	$\begin{bmatrix} 7 \times 7 \text{ Depth-wise conv, 512} \\ 7 \times 7 \text{ Depth-wise conv, } r=3, 512 \\ 1 \times 1, 2048 \\ 1 \times 1, 512 \end{bmatrix} \times 2$

channel number of later groups gradually becomes higher when the spatial size of features shrinks. Therefore, we propose the focal block to enlarge the receptive field of neurons in the last block group of each stage as an alternative way.

Two designs of the focal block are presented in Figure 5. A dilated *depth-wise* convolution and two skip connections are introduced to both the ConvNeXt block and the Swin Transformer block. Therefore, the focal block can incorporate both fine-grained local and coarse-grained global interactions simultaneously (where the name *focal block* comes from). Using global attention [38, 39] or large convolution kernels [5, 40] to enlarge the receptive field has been widely studied recently. Although achieving promising results, it usually introduces much computational cost and memory overhead when applying those operations to dense prediction tasks due to the large input image size. In contrast, the proposed focal block introduces marginal additional cost (See Table 9 in the Section 4.5 for comparison).

3.4. Architecture variants

We construct three CFNet variants, *i.e.* CFNet-T (Swin), CFNet-T (NeXt), and CFNet-S (NeXt). T and S are the abbreviations of the two words *tiny* and *small*, respectively, indicating the model size. The first one uses the Swin Transformer block and the focal Swin block. The other two use the ConvNeXt block and the focal NeXt block. The detailed configurations for each CFNet variant are shown in Table 1. The number of stages is set to 3 and 4 for CFNet-T and CFNet-S, respectively. Although different stages with different configurations may achieve better performance, we set the same configurations for all stages for simplicity. And the dilation rate r in all focal blocks is set to 3 by default. We do not consider bigger CFNet variants in this paper due to the limitation of computational resources.

Table 2. Empirical analysis on the supposition. Prop. denotes the proportion of parameters allocated for feature fusion. n_i^1, n_i^2, n_i^3 denote the number of blocks in the three block groups of the i -th stage. Acc denotes the top-1 classification accuracy on ImageNet.

Prop.	n_1^1, n_1^2, n_1^3	n_2^1, n_2^2, n_2^3	Param.	FLOPs	Acc	mAP
0	6, 9, 3	-	32.5M	5.34G	80.7	40.6
1/6	5, 10, 5	1, 2, 1	32.6M	5.58G	80.3	42.2
2/6	4, 8, 4	2, 4, 2	32.6M	5.58G	80.5	42.4
3/6	3, 6, 3	3, 6, 3	32.6M	5.58G	81.2	42.9
4/6	2, 4, 2	4, 8, 4	32.6M	5.58G	81.3	43.3
5/6	1, 2, 1	5, 10, 5	32.6M	5.58G	81.2	43.3

4. Experiments

4.1. Empirical analysis on the supposition

To validate our supposition that *allocating a larger proportion of parameters for feature fusion can achieve better performance*, we constructed several CFNet models with two stages, and controlled the parameters allocated for each stage by adjusting the number of blocks while keeping a similar model size. All models used the ConvNeXt block and the focal NeXt block. Because all these models have two stages, the proportion of parameters for feature fusion is the ratio of parameters of the second stage to the whole backbone according to the definition in Section 1. If the proportion is zero, CFNet degenerates to a structure similar to FPN. For simplicity, we calculated the proportions without considering the parameters (fewer than 0.5M) introduced by the stem and N blocks before the CFNet stages.

We pre-trained all backbones on ImageNet-1K [41] for 100 epochs, and fine-tuned the detector RetinaNet [11] on COCO [42] for 12 epochs. The other training details are

described in Section 4.2 and Section 4.3. The results in Table 2 and Figure 2 show that the detection performance (mAP) becomes better and saturated when the second stage becomes heavier, which indicates that allocating more parameters to fuse features can boost the detection performance. *This validates our supposition.* Here, we calculate the parameters and GFLOPs of the classification models for simplicity, which is the same as in Table 7-10 below.

Note that although the two stage CFNet models that allocate proper proportion of parameters for feature fusion performed well, in our final CFNet variants, we keep the same size for all stages to maintain a simple design and use more stages to achieve more effective feature fusion.

4.2. Image classification on ImageNet-1K

Although CFNet is proposed for dense prediction tasks, it can still benefit from large-scale pre-training due to its simple architecture. In this section, we present the image classification results of the CFNet models. It is worth noting that because CFNet does not need the extra fusion module (also named neck) used by its counterparts when applied to downstream tasks, the CFNet backbones (of models in Table 3 and Table 4) are allocated with slightly more parameters than their counterparts to compensate for that.

Settings. The ImageNet-1K dataset consists of 1000 object classes with 1.2M training images. We report the top-1 accuracy on the validation set following [5, 6]. To perform image classification, we removed the last transition block in CFNet models, and attached an FC head on C5 (the coarse scale features with a stride of 32 output by the last stage). Strictly following the settings used by [5], we trained the CFNet models for 300 epochs using AdamW [43] with a learning rate of 4e-3 by default to compare with other methods. There was a 20-epoch linear warmup and a cosine decaying schedule afterward. We used a batch size of 4096 and a weight decay of 0.05. For data augmentations, we adopted the common schemes including Mixup [44], Cutmix [45], RandAugment [46], and Random Erasing [47]. We regularized the networks with Stochastic Depth [48] and Label Smoothing [49]. Layer Scale [50] of initial value 1e-6 was applied. We also used Exponential Moving Average (EMA) [51] following [5].

Main results. Table 3 shows the results of CFNet models to compare with the baseline models and some recently proposed methods. CFNet-T (Swin), CFNet-T (NeXt), CFNet-S (NeXt) outperformed the baselines Swin-T, ConvNeXt-T, ConvNeXt-S by 1.3%, 1.0%, 0.8%, respectively. Because the CFNet models would be applied to downstream tasks without using extra fusion modules (e.g. the fusion modules used by FPN and its variants), we constructed the classification models with a slightly larger size than their baselines in order to keep comparable parameters and GFLOPs in downstream tasks. In spite of that, CFNet-T (NeXt) and CFNet-S

Table 3. Results of image classification on ImageNet-1K val. All models were trained and evaluated on 224×224 resolution.

Backbone	Param.	FLOPs	Top-1 Acc	Reference
Focal-T [7]	29.1M	4.9G	82.2	NeurIPS 2021
MViTv2-T [52]	24.0M	4.7G	82.3	CVPR 2022
CSwin-T [9]	23.0M	4.3G	82.7	CVPR 2022
MSG-T [53]	25.0M	3.8G	82.4	CVPR 2022
Swin-T [6]	28.3M	4.4G	81.2	ICCV 2021
ConvNeXt-T [5]	28.6M	4.5G	82.1	CVPR 2022
CFNet-T (Swin)	32.2M	5.8G	82.5	
CFNet-T (NeXt)	33.8M	5.7G	83.1	
Swin-S [6]	49.9M	8.7G	83.1	ICCV 2021
Focal-S [7]	51.1M	9.1G	83.5	NeurIPS 2021
MViTv2-S [52]	35.0M	7.0G	83.6	CVPR 2022
CSwin-S [9]	35.0M	6.9G	83.6	CVPR 2022
MSG-S [53]	56.0M	8.4G	83.4	CVPR 2022
ConvNeXt-S [5]	50.2M	8.7G	83.1	CVPR 2022
CFNet-S (NeXt)	55.1M	9.8G	83.9	
Swin-B [6]	87.8M	15.4G	83.4	ICCV 2021
Focal-B [7]	89.8M	16.0G	83.8	NeurIPS 2021
ConvNeXt-B [5]	89.0M	15.4G	83.8	CVPR 2022

(NeXt) even achieved comparable performance to the larger models ConvNeXt-S and ConvNeXt-B, respectively.

4.3. Object detection on COCO

Settings. We benchmark our models on object detection and instance segmentation with COCO 2017 [42] based on three representative pipelines, *i.e.* RetinaNet [11], Mask R-CNN [10], and Cascade Mask R-CNN [54] using the MMDetection [55] toolboxes. We used the final model weights (instead of the EMA weights) from ImageNet pre-training as network initialization. All detectors were fine-tuned on the 118k training images, and we report the results on the 5k validation set. For training settings, we mainly followed ConvNeXt [5] and Swin Transformer [6]. Specifically, we used AdamW [43] for optimization and set the weight decay to 0.95. All models were trained by 3× schedule, with a batch size of 16 and an initial learning rate of 0.0001. We found that the proposed CFNet models were easy to overfit the training data. To fully explore the capacity of CFNet models, we used large scale jittering during training following [56], *i.e.* we randomly resized the input image with a scale ratio range of [0.1, 2.0], and then cropped a patch of 1024×1024. We also used the copy-and-paste data augmentation proposed in [56], but only with box annotations. *Note that we re-trained all baseline models with the same data augmentations for fair comparison.*

Main results. Table 4 presents the object detection and instance segmentation results of the CFNet models to compare with the baseline models and some recently developed

Table 4. Results of object detection on COCO *val2017*. We did not use extra feature fusion module when applying the CFNet models to detectors. We took an input image size of 1280×800 pixels to calculate the model parameters and GFLOPs following [5].

(a) RetinaNet								
Backbone	Param	FLOPs	AP^b	AP_{50}^b	AP_{75}^b	AP_S^b	AP_M^b	AP_L^b
Swin-T [6]	39M	245G	45.0	65.9	48.4	29.7	48.9	58.1
ConvNeXt-T [5]	39M	243G	45.2	65.7	48.5	28.8	49.3	58.9
Focal-T [7]	39M	265G	45.5	66.3	48.8	31.2	49.2	58.7
Swin-S [6]	60M	335G	46.4	67.0	50.1	31.0	50.1	60.3
Focal-S [7]	62M	367G	47.3	67.8	51.0	31.6	50.9	61.1
Swin-T	39M	245G	44.9	66.1	48.1	30.5	49.0	59.3
CFNet-T (Swin)	37M	262G	47.4	68.9	50.5	33.1	51.5	61.7
ConvNeXt-T	39M	243G	45.4	67.0	48.7	29.5	49.9	59.9
CFNet-T (NeXt)	39M	255G	48.3	69.1	51.6	33.2	53.1	62.7
ConvNeXt-S	60M	329G	47.4	68.3	51.2	32.0	51.5	61.6
CFNet-S (NeXt)	61M	335G	49.6	70.8	53.2	34.8	54.0	63.5
(b) Mask R-CNN								
Backbone	Param	FLOPs	AP^b	AP_{50}^b	AP_{75}^b	AP^m	AP_{50}^m	AP_{75}^m
Swin-T [6]	48M	264G	46.0	68.1	50.3	41.6	65.1	44.9
ConvNeXt-T [5]	48M	262G	46.2	67.9	50.8	41.7	65.0	44.9
Focal-T [7]	49M	291G	47.2	69.4	51.9	42.7	66.5	45.9
MViTv2-T [52]	44M	279G	48.2	70.9	53.3	43.8	67.9	47.2
CSwin-T [9]	42M	279G	49.0	70.7	53.7	43.6	67.9	46.6
Swin-S [6]	69M	354G	48.5	70.2	53.5	43.3	67.3	46.6
Focal-S [7]	71M	401G	48.8	70.5	53.6	43.8	67.7	47.2
MViTv2-S [52]	54M	326G	49.9	72.0	55.0	45.1	69.5	48.5
CSwin-S [9]	54M	342G	50.0	71.3	54.7	44.5	68.4	47.7
Swin-T	48M	264G	46.3	68.6	51.0	42.3	65.8	46.0
CFNet-T (Swin)	48M	281G	48.3	70.5	52.9	43.8	67.4	47.5
ConvNeXt-T	48M	262G	46.4	68.1	51.3	42.3	65.2	45.9
CFNet-T (NeXt)	49M	274G	49.2	70.3	53.7	44.1	67.8	47.5
ConvNeXt-S	70M	348G	48.5	70.0	53.3	43.8	67.2	47.7
CFNet-S (NeXt)	72M	355G	50.4	71.7	55.1	45.0	68.9	48.6
(c) Cascade Mask R-CNN								
Backbone	Param	FLOPs	AP^b	AP_{50}^b	AP_{75}^b	AP^m	AP_{50}^m	AP_{75}^m
Swin-T [6]	86M	745G	50.5	69.3	54.9	43.7	66.6	47.1
ConvNeXt-T [5]	86M	741G	50.4	69.1	54.8	43.7	66.5	47.3
MSG-T [53]	83M	731G	51.4	70.1	56.0	44.6	67.4	48.1
MViTv2-T [52]	76M	701G	52.2	71.1	56.6	45.0	68.3	48.9
CSwin-T [9]	80M	757G	52.5	71.5	57.1	45.3	68.8	48.9
Swin-S [6]	107G	838G	51.8	70.4	56.3	44.7	67.9	48.5
ConvNeXt-S [6]	108M	827G	51.9	70.8	56.5	45.0	68.4	49.1
MSG-S [53]	113M	831G	52.5	71.1	57.2	45.5	68.4	49.5
MViTv2-S [52]	87M	748G	53.2	72.4	58.0	46.0	69.6	50.1
CSwin-S [9]	90M	820G	53.7	72.2	58.4	46.4	69.6	50.6
Swin-T	86M	745G	50.7	69.6	55.0	44.4	67.2	48.2
CFNet-T (Swin)	86M	760G	52.0	70.8	56.3	45.5	68.5	49.6
ConvNeXt-T	86M	741G	50.8	69.4	55.2	44.5	66.9	48.5
CFNet-T (NeXt)	87M	753G	52.5	71.4	56.8	45.9	69.0	49.7
ConvNeXt-S	108M	827G	51.9	71.0	56.6	45.4	68.6	49.5
CFNet-S (NeXt)	110M	833G	53.5	72.4	58.1	46.7	69.9	50.6

methods that achieve strong performance. Across different model complexity and different detectors, the CFNet models yielded significant gains over the baselines. The model

Table 5. Comparison with FPN and its variants. All models were fine-tuned by 3× schedule under the same training setting. The FPS was measured using a single Nvidia RTX 3090 GPU.

Backbone	Fusion Module	Param.	FLOPs	AP^{box}	Memory	FPS ↑
ConvNeXt-T	FPN [14]	39M	243G	45.4	6.3G	19
ConvNeXt-T	BiFPN [17]	39M	248G	46.7	8.1G	15
ConvNeXt-T	NAS-FPN [16]	47M	289G	46.6	6.9G	17
ConvNeXt-T	PAFPN [15]	61M	315G	47.0	7.2G	16
CFNet-T (NeXt)	-	39M	255G	48.3	8.2G	16

CFNet-T (NeXt) even achieved 2.9, 2.8, 1.7 box AP improvements over the ConvNeXt-T based on the three detectors, respectively. When scaled up to the bigger model CFNet-S (NeXt), CFNet still outperformed its baseline by 1.6 box AP and 1.3 mask AP based on the powerful Cascade Mask R-CNN. *It is worth noting that the block used in CFNet can be freely replaced with any designs proposed in previous works. For example, by using the more powerful CSWin Transformer block to construct CFNet-T, it achieved 50.4 box AP and 45.2 mask AP based on the Mask R-CNN, significantly outperforming the CSWin-T.*

Comparison with FPN and its variants. We conducted experiments on the ConvNeXt-T model combined with different fusion modules based on RetinaNet to compare with CFNet-T (NeXt). For BiFPN [17], we implemented it by adding six pairs of top-down and bottom-up pathways after the backbone following the original paper to keep a similar model size as FPN. For NAS-FPN [16] and PAFPN [15], we implemented both by adding three repeated stages after the backbone based on MMDetection [55]. The results in Table 5 show that CFNet outperformed FPN and its variants significantly while keeping similar (training) memory cost and competitive inference speed (see the metric FPS, the higher, the better), which indicates the superiority of CFNet to extract multi-scale features.

4.4. Semantic segmentation on ADE20k

Settings. We conducted experiments on semantic segmentation with ADE20k [57] based on UperNet [13] using the MMsegmentation [58] toolboxes, and report the results on the 2k validation set. As the FPN used in UperNet includes a heavy top-down pathway, we merely replaced the classification backbone but maintained the rest parts when applying our CFNet to UperNet (by removing the last transition block), in order to keep a similar model size to the baseline models. The input images were resized and randomly cropped into 512×512 patches strictly following [5, 6]. As the data augmentations used for semantic segmentation are strong enough to train the proposed CFNet models, no extra data augmentations were introduced. All model variants were trained for 160k with a batch size of 16 and an initial learning rate of 0.0001.

Table 6. Results of semantic segmentation on ADE20K *validation* set using UperNet [13]. The superscripts *ss* and *ms* denote single-scale and multi-scale testing, respectively.

Backbone	Param.	FLOPs	Input size	mIoU ^{ss}	mIoU ^{ms}
Focal-T [7]	62M	998G	512 ²	45.5	47.0
Swin-S [6]	81M	1038G	512 ²	47.6	49.5
Focal-S [7]	85M	1130G	512 ²	48.0	50.0
Swin-B [6]	121M	1188G	512 ²	48.1	49.7
ConvNeXt-B [5]	122M	1170G	512 ²	49.1	49.9
Swin-T [6]	60M	945G	512 ²	44.5	45.8
CFNet-T (Swin)	59M	970G	512 ²	46.3	47.7
ConvNeXt-T [5]	60M	939G	512 ²	46.0	46.7
CFNet-T (NeXt)	61M	962G	512 ²	47.6	48.9
ConvNeXt-S [5]	82M	1027G	512 ²	48.7	49.6
CFNet-S (NeXt)	83M	1045G	512 ²	49.1	50.4

Main results. Table 6 presents the semantic segmentation results. Compared with the baselines, CFNet achieved 0.7-2.1 mIoU improvements with different model variants, which indicates the generalization ability of our method.

4.5. Ablation studies

To better understand CFNet, we ablated some key components and evaluated the performance on both classification and object detection based on CFNet-T (NeXt) and RetinaNet. For experiments in Table 7 and Table 8, we first pre-trained the CFNet backbones on ImageNet-1K for 100 epochs, and then fine-tuned the detectors on COCO by 1× schedule. For experiments in Table 9 and Table 10, we pre-trained the backbones for 300 epochs and fine-tuned the detectors by 3× schedule to make sure models converged.

Different number of stages. We constructed the model CFNet-T (NeXt) with different number of stages, and all stages shared the same configurations. More stages indicate more parameters can be utilized to fuse multi-scale features. The results in Table 7 show that the CFNet-T (NeXt) model with three stages achieved the best performance. Intuitively, the CFNet model with more stages can achieve feature fusion more sufficiently, but the more complicated topological connections may make it harder to optimize.

Different fusion blocks. We conducted experiments on the CFNet-T (NeXt) models with different fusion blocks, and the results are presented in Table 8. The ‘Sequentially Add’ fusion achieved slightly better performance than the ‘Concat’ fusion with fewer GFLOPs. Both of them outperformed the ‘Add’ Fusion by a large margin. We believe that better transition block (*e.g.* attention guided integration [18]) can further boost the final performance.

Effectiveness of the focal block. Table 9 shows the ablation results of the focal block. Although the model with focal block did not achieve a better classification accuracy, it

Table 7. Different number of stages. n_i^1, n_i^2, n_i^3 denote the number of blocks in the three block groups of the i -th stage, respectively.

Number of stage	n_i^1, n_i^2, n_i^3	Param.	FLOPs	Acc	mAP
1	6, 9, 3	32.5M	5.34G	80.7	40.6
2	3, 6, 3	32.6M	5.58G	81.2	42.9
3	2, 4, 2	33.8M	5.70G	81.0	43.3
4	1, 4, 1	34.2M	5.91G	81.2	43.1

Table 8. Different fusion blocks. Seq. denotes ‘Sequentially’.

Backbone	Transition block	Param.	FLOPs	Acc	mAP
CFNet-T (NeXt)	Add	33.7M	5.75G	80.6	42.4
CFNet-T (NeXt)	Concat	33.7M	5.97G	81.0	43.0
CFNet-T (NeXt)	Seq. Add	33.8M	5.70G	81.0	43.3

Table 9. Effectiveness of the focal block.

Backbone	Focal block	Param.	FLOPs	Acc	mAP
CFNet-T (NeXt)		33.7M	5.69G	83.1	47.9
CFNet-T (NeXt)	✓	33.8M	5.70G	83.1	48.3

Table 10. Influence of the stronger data augmentations.

Backbone	Stronger aug.	AP ^b	AP ₅₀ ^b	AP ₇₅ ^b
ConvNeXt-T		45.2	65.7	48.5
ConvNeXt-T	✓	45.4 (+0.2)	66.5	48.7
CFNet-T (NeXt)		47.0	67.8	50.4
CFNet-T (NeXt)	✓	48.3 (+1.3)	69.1	51.6

boosted the detection performance by 0.4 AP over its counterpart. This might be because the detectors with larger input image size need larger receptive field than classification models. It is worth noting that the focal block is only applied to the last block group of each stage, and it introduces marginal additional cost (less than 1%).

Influence of the stronger data augmentations. We compared the data augmentations used by previous works [5, 6] and the stronger data augmentations we used on detection fine-tuning. As presented in Table 10, the ConvNeXt models achieved similar performance on both settings, but the CFNet model achieved significantly better performance with the stronger data augmentations. We conjecture that this might be because CFNet has a higher capacity than ConvNeXt. Therefore, the data augmentations used for training ConvNeXt models are not strong enough to fully explore the power of the CFNet models.

5. Further analysis

We tried to analyze the differences between the proposed CFNet and its baselines more deeply by comparing their in-

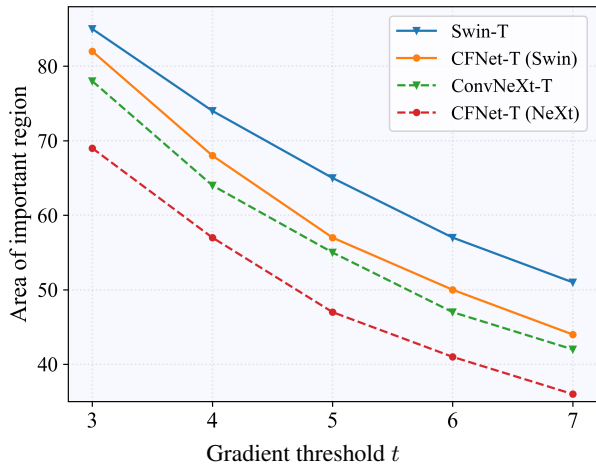


Figure 6. Comparison on the average area of *important regions* generated from different models with different gradient thresholds. We normalized the values of both axes for better visualization.

put gradient distributions. Specifically, we focus on the images in the validation set where the CFNet models achieved the most improvements over the baselines. We fed the selected images into the trained models and performed the backward process to acquire the input gradient maps with a spatial size same as the input images. For each image, we define the *important region* as the region where the gradient is greater than t , and t is a threshold to adjust the size of the important region.

How to acquire the target images? For every annotated object in an image, we first acquired the detection result with maximum IoU. If there is no matched result for a specific object, we added a virtual matched result for it and set both the IoU and confidence score of the matched result to zero. We then calculated the *detection quality score* of each annotated object by multiplying the IoU and confidence score of the matched result. The detection quality score of an image was the average quality score of all objects in the image. Finally, we could get the top- k images where the CFNet models achieved the most improvements according to the image detection quality scores.

Results. We compared the CFNet (NeXt) model with its baseline based on RetinaNet by selecting the top-1000 images. The visualizations in Figure 7 show that the CFNet model concentrates more on regions inside objects with more discriminative boundaries, and predicts more precise bounding box with higher confidence. In some cases (e.g. image (d)-(f)), the IoU of the boxes predicted by the CFNet model is similar to that predicted by the ConvNeXt model, but the confidence of those boxes predicted by the CFNet model is higher than the latter. The higher confidence of true positives is more likely to lead to higher mAP because

the confidence of predicted boxes decides the ranking when calculating the precision-recall curve.

In addition, we calculated the average area of important regions with different gradient thresholds on those selected images. The statistical results in Figure 6 show that the average area of important regions generated from the CFNet models is smaller than that generated from the baseline models, indicating that the CFNet models concentrate on smaller regions.

6. Conclusion

In this paper, we present a novel architecture named CFNet for dense prediction tasks. Different from the widely used FPN and its variants, which usually use a lightweight fusion module to fuse the multi-scale features extracted by a heavy classification backbone, the proposed CFNet introduces several cascaded stages to learn multi-scale representations based on the extracted high-resolution features. Through inserting the feature integration operation into the backbone, a large proportion of the whole backbone can be utilized to fuse the multi-scale features effectively. We conducted extensive experiments on several popular dense prediction tasks to validate the effectiveness of our method.

Acknowledgements. We thank Chufeng Tang, Junru Tan, Kai Li, Hang Chen, Junnan Chen for valuable discussions and feedback. This work was supported by the National Natural Science Foundation of China (Nos. 62061136001, U19B2034, 61836014) and THU-Bosch JCML center.

Appendix

A1. Comparison with the backbone related methods

We have compared CFNet with the recent works that adopt FPN and its variants to perform feature fusion in Table 4 and Table 5. For those methods which adopt multi-scale feature fusion in backbone, because the training settings they used are different from the recent works published after the ViT [38], we give a rough comparison with them below.

Table 11. Rough comparison with methods that adopt multi-scale feature fusion in backbone.

Model	Detectors	Param.	AP ^b	AP ^m
ResNet-101 w/ FPN	HTC	99M	44.9	39.4
HRNet-w32 w/ FPN	HTC	86M	45.3	39.6
DectectRS-ResNet-50	HTC	105M	46.2	40.4
CBNet-ResNeXt-152	Cascade Mask R-CNN	287M	50.7	43.3
ConvNeXt-T w/ FPN	Cascade Mask R-CNN	86M	50.8	44.5
CFNet-T (NeXt)	Cascade Mask R-CNN	87M	52.5	45.9

References

- [1] Alex Krizhevsky, Ilya Sutskever, and Geoffrey E Hinton. Imagenet classification with deep convolutional neural networks. In *NeurIPS*, 2012. 1

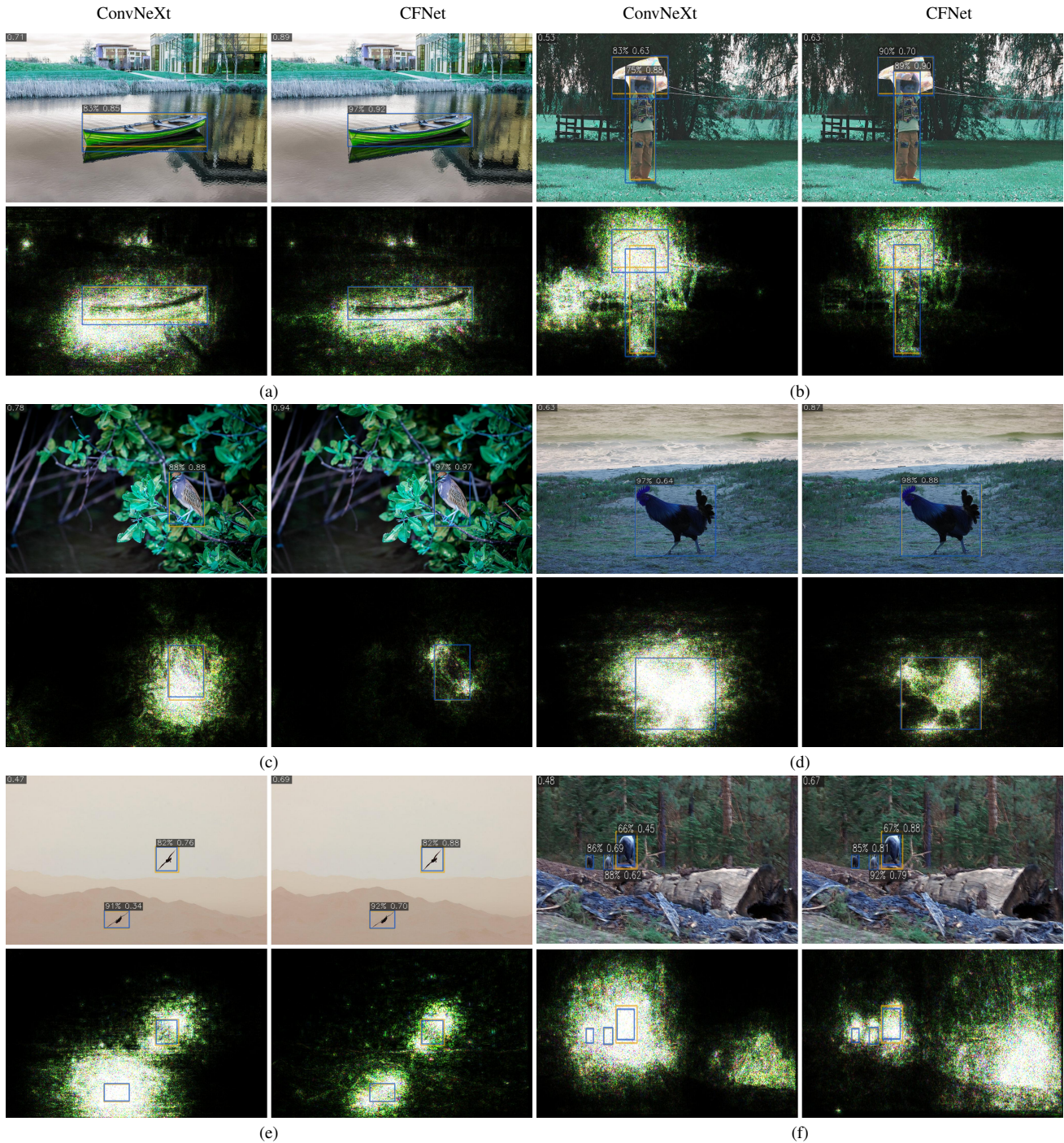


Figure 7. Detection results (top row) and input gradient maps (bottom row) of ConvNeXt (left column) and CFNet (right column). The orange and blue boxes are human-annotated boxes and predicted boxes, respectively. The score pair (iou, confidence) is provided above each predicted box. The image detection quality score is displayed in the upper left corner of each image. The brighter the color in the gradient maps, the higher the gradient. Please zoom in for more clear details.

[2] Karen Simonyan and Andrew Zisserman. Very deep convolutional networks for large-scale image recognition. In *ICLR*, 2015. 1

[3] Christian Szegedy, Wei Liu, Yangqing Jia, Pierre Sermanet,

Scott Reed, Dragomir Anguelov, Dumitru Erhan, Vincent Vanhoucke, and Andrew Rabinovich. Going deeper with convolutions. In *CVPR*, 2015. 1

[4] Kaiming He, Xiangyu Zhang, Shaoqing Ren, and Jian Sun.

- Deep residual learning for image recognition. In *CVPR*, 2016. 1, 2, 3
- [5] Zhuang Liu, Hanzi Mao, Chao-Yuan Wu, Christoph Feichtenhofer, Trevor Darrell, and Saining Xie. A convnet for the 2020s. In *CVPR*, 2022. 1, 2, 4, 5, 6, 7, 8
- [6] Ze Liu, Yutong Lin, Yue Cao, Han Hu, Yixuan Wei, Zheng Zhang, Stephen Lin, and Baining Guo. Swin transformer: Hierarchical vision transformer using shifted windows. In *ICCV*, 2021. 1, 2, 4, 6, 7, 8
- [7] Jianwei Yang, Chunyuan Li, Pengchuan Zhang, Xiyang Dai, Bin Xiao, Lu Yuan, and Jianfeng Gao. Focal self-attention for local-global interactions in vision transformers. In *NeurIPS*, 2021. 1, 6, 7, 8
- [8] Weihao Yu, Mi Luo, Pan Zhou, Chenyang Si, Yichen Zhou, Xinchao Wang, Jiashi Feng, and Shuicheng Yan. Metaformer is actually what you need for vision. In *CVPR*, 2022. 1
- [9] Xiaoyi Dong, Jianmin Bao, Dongdong Chen, Weiming Zhang, Nenghai Yu, Lu Yuan, Dong Chen, and Baining Guo. Cswin transformer: A general vision transformer backbone with cross-shaped windows. In *CVPR*, 2022. 1, 6, 7
- [10] Kaiming He, Georgia Gkioxari, Piotr Dollar, and Ross Girshick. Mask R-CNN. In *ICCV*, 2017. 1, 2, 6
- [11] Tsung-Yi Lin, Priya Goyal, Ross Girshick, Kaiming He, and Piotr Dollar. Focal loss for dense object detection. In *ICCV*, 2017. 1, 4, 5, 6
- [12] Zhi Tian, Chunhua Shen, Hao Chen, and Tong He. FCOS: Fully convolutional one-stage object detection. In *ICCV*, 2019. 1, 4
- [13] Tete Xiao, Yingcheng Liu, Bolei Zhou, Yuning Jiang, and Jian Sun. Unified perceptual parsing for scene understanding. In *ECCV*, 2018. 1, 2, 7, 8
- [14] Tsung-Yi Lin, Piotr Dollar, Ross Girshick, Kaiming He, Bharath Hariharan, and Serge Belongie. Feature pyramid networks for object detection. In *CVPR*, 2017. 1, 3, 7
- [15] Shu Liu, Lu Qi, Haifang Qin, Jianping Shi, and Jiaya Jia. Path aggregation network for instance segmentation. In *CVPR*, 2018. 1, 3, 4, 7
- [16] Golnaz Ghiasi, Tsung-Yi Lin, Ruoming Pang, and Quoc V. Le. Nas-fpn: Learning scalable feature pyramid architecture for object detection. In *CVPR*, 2019. 1, 3, 4, 7
- [17] Mingxing Tan, Ruoming Pang, and Quoc V. Le. Efficientdet: Scalable and efficient object detection. In *CVPR*, 2020. 1, 3, 4, 7
- [18] Miao Hu, Yali Li, Lu Fang, and Shengjin Wang. A2-fpn: Attention aggregation based feature pyramid network for instance segmentation. In *CVPR*, 2021. 1, 3, 8
- [19] Tiancai Wang, Xiangyu Zhang, and Jian Sun. Implicit feature pyramid network for object detection. *CoRR*, abs/2012.13563, 2020. 1
- [20] Alexander Kirillov, Ross Girshick, Kaiming He, and Piotr Dollar. Panoptic feature pyramid networks. In *CVPR*, 2019. 1
- [21] Olaf Ronneberger, Philipp Fischer, and Thomas Brox. U-net: Convolutional networks for biomedical image segmentation. In *MICCAI*, 2015. 2
- [22] Vijay Badrinarayanan, Ankur Handa, and Roberto Cipolla. Segnet: A deep convolutional encoder-decoder architecture for robust semantic pixel-wise labelling. *CoRR*, abs/1505.07293, 2015. 2
- [23] Alejandro Newell, Kaiyu Yang, and Jia Deng. Stacked hourglass networks for human pose estimation. In *ECCV*, 2016. 2
- [24] Zeming Li, Chao Peng, Gang Yu, Xiangyu Zhang, Yangdong Deng, and Jian Sun. Detnet: Design backbone for object detection. In *ECCV*, 2018. 2
- [25] Jingdong Wang, Ke Sun, Tianheng Cheng, Borui Jiang, Chaorui Deng, Yang Zhao, Dong Liu, Yadong Mu, Mingkui Tan, Xinggang Wang, Wenyu Liu, and Bin Xiao. Deep high-resolution representation learning for visual recognition. *TPAMI*, 2019. 2, 3
- [26] Xianzhi Du, Tsung-Yi Lin, Pengchong Jin, Golnaz Ghiasi, Mingxing Tan, Yin Cui, Quoc V. Le, and Xiaodan Song. Spinenet: Learning scale-permuted backbone for recognition and localization. In *CVPR*, 2020. 2, 3
- [27] Yudong Liu, Yongtao Wang, Siwei Wang, Tingting Liang, Qijie Zhao, Zhi Tang, and Haibin Ling. Cbnet: A novel composite backbone network architecture for object detection. In *AAAI*, 2020. 2, 3
- [28] Siyuan Qiao, Liang-Chieh Chen, and Alan Yuille. Detectors: Detecting objects with recursive feature pyramid and switchable atrous convolution. In *CVPR*, 2021. 2, 3
- [29] Yiqi Jiang, Zhiyu Tan, Junyan Wang, Xiuyu Sun, Ming Lin, and Hao Li. Giraffedet: A heavy-neck paradigm for object detection. In *ICLR*, 2022. 2, 3
- [30] Barret Zoph and Quoc V. Le. Neural architecture search with reinforcement learning. In *ICLR*, 2017. 3
- [31] Liang-Chieh Chen, Yukun Zhu, George Papandreou, Florian Schroff, and Hartwig Adam. Encoder-decoder with atrous separable convolution for semantic image segmentation. In *ECCV*, 2018. 3
- [32] Tianjian Meng, Golnaz Ghiasi, Reza Mahjorian, Quoc V Le, and Mingxing Tan. Revisiting multi-scale feature fusion for semantic segmentation. In *arXiv:2203.12683*, 2022. 3
- [33] Dong Zhang, Zhang Hanwang, Tang Jinhui, Meng Wang, Hua Xiansheng, and Sun Qianru. Feature pyramid transformer. In *ECCV*, 2020. 3
- [34] Geoffrey E. Hinton Jimmy Lei Ba, Jamie Ryan Kiros. Layer normalization. In *arXiv:1607.06450*., 2016. 3, 4
- [35] Dan Hendrycks and Kevin Gimpel. Gaussian error linear units (gelus). In *arXiv:1606.08415*., 2016. 3, 4
- [36] Shifeng Zhang, Cheng Chi, Yongqiang Yao, Zhen Lei, and Stan Z. Li. Bridging the gap between anchor-based and anchor-free detection via adaptive training sample selection. In *CVPR*, 2020. 4

- [37] Xiang Li, Wenhai Wang, Xiaolin Hu, Jun Li, Jinhui Tang, and Jian Yang. Generalized focal loss v2: Learning reliable localization quality estimation for dense object detection. In *CVPR*, 2021. 4
- [38] Alexey Dosovitskiy, Lucas Beyer, Alexander Kolesnikov, Dirk Weissenborn, Xiaohua Zhai, Thomas Unterthiner, Mostafa Dehghani, Matthias Minderer, Georg Heigold, Sylvain Gelly, Jakob Uszkoreit, and Neil Houlsby. An image is worth 16x16 words: Transformers for image recognition at scale. In *ICLR*, 2021. 5, 9
- [39] Yongming Rao, Wenliang Zhao, Zheng Zhu, Jiwen Lu, and Jie Zhou. Global filter networks for image classification. In *NeurIPS*, 2021. 5
- [40] Xiaohan Ding, Xiangyu Zhang, Jungong Han, and Guiguang Ding. Scaling up your kernels to 31x31: Revisiting large kernel design in cnns. In *CVPR*, 2022. 5
- [41] J. Deng, W. Dong, R. Socher, L.-J. Li, K. Li, and L. Fei-Fei. ImageNet: A large-scale hierarchical image database. In *CVPR*, 2009. 5
- [42] Tsung-Yi Lin, Michael Maire, Serge Belongie, James Hays, Pietro Perona, Deva Ramanan, Piotr Dollár, and C. Lawrence Zitnick. Microsoft COCO: Common objects in context. In *ECCV*, 2014. 5, 6
- [43] Diederik P. Kingma and Jimmy Ba. Adam: A method for stochastic optimization. In *ICLR*, 2015. 6
- [44] Hongyi Zhang, Moustapha Cisse, Yann N. Dauphin, and David Lopez-Paz. mixup: Beyond empirical risk minimization. In *ICLR*, 2018. 6
- [45] Sangdoon Yun, Dongyoon Han, Seong Joon Oh, Sanghyuk Chun, Junsuk Choe, and Youngjoon Yoo. Cutmix: Regularization strategy to train strong classifiers with localizable features. In *ICCV*, 2019. 6
- [46] Ekin Dogus Cubuk, Barret Zoph, Jon Shlens, and Quoc Le. Randaugment: Practical automated data augmentation with a reduced search space. In *NIPS*, 2020. 6
- [47] Zhun Zhong, Liang Zheng, Guoliang Kang, Shaozi Li, and Yi Yang. Random erasing data augmentation. 2020. 6
- [48] Gao Huang, Yu Sun, Zhuang Liu, Daniel Sedra, and Kilian Q. Weinberger. Deep networks with stochastic depth. In *ECCV*, 2016. 6
- [49] Christian Szegedy, Vincent Vanhoucke, Sergey Ioffe, Jon Shlens, and Zbigniew Wojna. Rethinking the inception architecture for computer vision. In *CVPR*, 2016. 6
- [50] Hugo Touvron, Matthieu Cord, Alexandre Sablayrolles, Gabriel Synnaeve, and Hervé Jégou. Going deeper with image transformers. In *ICCV*, 2021. 6
- [51] Polyak Boris T and Juditsky Anatoli B. Acceleration of stochastic approximation by averaging. *SIAM Journal on Control and Optimization*, 1992. 6
- [52] Yanghao Li, Chao-Yuan Wu, Haoqi Fan, Karttikeya Mangalam, Bo Xiong, Jitendra Malik, and Christoph Feichtenhofer. Mvity2: Improved multiscale vision transformers for classification and detection. In *CVPR*, 2022. 6, 7
- [53] Jiemin Fang, Lingxi Xie, Xinggang Wang, Xiaopeng Zhang, Wenyu Liu, and Qi Tian. Msg-transformer: Exchanging local spatial information by manipulating messenger tokens. In *CVPR*, 2022. 6, 7
- [54] Zhaowei Cai and Nuno Vasconcelos. Cascade r-cnn: Delving into high quality object detection. In *CVPR*, 2018. 6
- [55] Kai Chen, Jiaqi Wang, Jiangmiao Pang, Yuhang Cao, Yu Xiong, Xiaoxiao Li, Shuyang Sun, Wansen Feng, Zhiwei Liu, Jiarui Xu, Zheng Zhang, Dazhi Cheng, Chenchen Zhu, Tianheng Cheng, Qijie Zhao, Buyu Li, Xin Lu, Rui Zhu, Yue Wu, Jifeng Dai, Jingdong Wang, Jianping Shi, Wanli Ouyang, Chen Change Loy, and Dahua Lin. Mmdetection: Open mmlab detection toolbox and benchmark. *CoRR*, abs/1906.07155, 2019. 6, 7
- [56] Golnaz Ghiasi, Yin Cui, Aravind Srinivas, Rui Qian, Tsung-Yi Lin, Ekin D. Cubuk, Quoc V. Le, and Barret Zoph. Simple copy-paste is a strong data augmentation method for instance segmentation. In *CVPR*, 2021. 6
- [57] Bolei Zhou, Hang Zhao, Xavier Puig, Sanja Fidler, Adela Barriuso, and Antonio Torralba. Scene parsing through ade20k dataset. In *CVPR*, 2017. 7
- [58] MMSegmentation Contributors. MMSegmentation: Openmmlab semantic segmentation toolbox and benchmark. <https://github.com/open-mmlab/mmdetection>, 2020. 7